EXPERIMENTAL AND KINETIC MODELING STUDY OF METHANOL IGNITION AND OXIDATION AT HIGH PRESSURE

V. Aranda[a,b], J.M. Christensen[b], M.U. Alzueta[a], P. Glarborg[b], S. Gersen[c], Y. Gao[d], P. Marshall[d]

[a] Aragón Institute of Engineering Research (I3A), University of Zaragoza.

Campus Río Ebro, 50018 Zaragoza, Spain

[b] Department of Chemical and Biochemical Engineering, Technical University of Denmark, DK-2800 Lyngby, Denmark

[c] DNV KEMA Energy & Sustainability, P.O. Box 2029, 9704 CA Groningen, The Netherlands

[d] Department of Chemistry and Center for Advanced Scientific Computing and Modeling (CASCaM), University of North Texas, Denton, TX 76203-5070, USA

Abstract

A detailed chemical kinetic model for oxidation of CH_3OH at high pressure and intermediate temperatures has been developed and validated experimentally. Ab initio calculations and RRKM analysis were used to obtain rate coefficients for key reactions of CH_2OH and CH_3O (dissociation, isomerization, reaction with O_2). The experiments, involving CH_3OH/O_2 mixtures diluted in N_2, were carried out in a high pressure flow reactor at 600–900 K and 20-100 bar, varying the reaction stoichiometry from very lean to fuel-rich conditions. Under the conditions studied, the onset temperature for methanol oxidation was not dependent on the stoichiometry, while increasing pressure shifted the ignition temperature towards lower values. Model predictions of the present experimental results, as well as Rapid Compression Machine (RCM) data from the literature, were generally satisfactory. The governing reaction pathways have been outlined based on calculations with the kinetic model. Unlike what has been observed for unsaturated hydrocarbons, the oxidation

pathways for CH_3OH under the investigated conditions were very similar to those prevailing at higher temperatures and lower pressures. At the high pressures, the modeling predictions for onset of reaction were particularly sensitive to the $CH_3OH+HO_2 \rightleftharpoons CH_2OH+H_2O_2$ reaction.

Keywords

Methanol; oxidation; ignition; high pressure; flow reactor experiments; ab initio calculations

1. Introduction

Oxygenated organic compounds have been proposed as alternative fuels to diesel in order to improve the fuel properties and reduce particulates and NO_x emissions [1]. Methanol, which is the simplest alcohol, has been used in reformulated gasolines with significant success, and recently has also received attention for diesel engine applications. Its range of production sources and its chemical structure, with a high oxygen content and no C-C bonds, causes methanol to be one of the most important oxygenated additives. For these reasons, a number of studies have addressed the use of methanol-diesel blends in diesel engines [2-5]. Most of the authors conclude that the addition of methanol reduces the emissions of particulates and NO_x, even though some reported results seem contradictory.

Laboratory experiments allow more controlled conditions compared to tests in engines; methanol oxidation has been studied in flames [6-8], stirred reactors [9], static reactors [10, 11], flow reactors [12-15], Rapid Compression Machines [16], and shock tubes [17]. Of these studies, only three have been carried out at elevated pressures, i.e. 10 bar [9], 20 bar [13] and 30 bar [16], respectively. The aim of the present work is to investigate methanol oxidation at even higher pressures, which are of interest for combustion devices such as diesel engines. To achieve this, experiments were conducted

in a flow reactor at pressures of 20-100 bar and 600-900 K, as a function of stoichiometry. In addition, high pressure ignition delays, obtained in a Rapid Compression Machine [16], were taken into consideration. The results were analyzed in terms of an updated detailed chemical kinetic model. Selected reactions, potentially important at high pressure, were characterized from ab initio calculations over a wide range of pressure and temperature.

2. Experimental

Experiments have been conducted in a high pressure laminar flow reactor, described in detail elsewhere [18]. The quartz reactor, which has been designed to ensure a good plug approximation and a well-defined reaction volume (inside diameter 8 mm, outside diameter 10 mm, length 1545 mm), was enclosed in a stainless steel tube that acted as a pressure shell. A pressure control system delivered nitrogen to the shell-side of the reactor to obtain a pressure similar to that inside the reactor. The steel tube was placed horizontally in an oven with three individually controlled electrical heating elements that produced an isothermal reaction zone (±5 K) of approximately 40 cm. The reactor temperature was monitored by a type K thermocouple (±2.2 K) located inside a steel thermo pocket placed in the pressure shell. Reactant gases were fed into the system through high pressure differential mass flow controllers.

A liquid feeding system, described in greater detail elsewhere [19], was used to supply the methanol. The methanol was pressurized by an HPLC pump and its flow was controlled by a liquid mass flow controller. The liquid was evaporated at 250ºC. All the reactants were mixed before entering the reactor. Gas cylinder concentration certification was ≥ 99.998% for O_2 and N_2. The methanol, which was supplied by Sigma-Aldrich, had a purity of ≥ 99.8%.

The reactor pressure was monitored upstream of the reactor by a differential pressure transducer and controlled by a pneumatic pressure valve positioned after the reactor. At the outlet of the reactor, the pressure was reduced down to atmospheric pressure prior to analysis. A gas chromatograph, equipped with TCD and FID detectors, was used to measure CH_3OH, C_2H_5OH, CH_4, O_2, CO, and CO_2. The uncertainty of the measurements was estimated to be ±5%.

3. Chemical kinetic model

The mechanism used in the present study is based on the atmospheric pressure methanol schemes by the authors [14, 15], drawing also on previous high pressure work on oxidation of CO and CH_4 [18, 20, 21]. The methanol subset has been updated with results from recent theoretical work [22-24] and from ab initio calculations and RRKM analysis made as part of the present work on reactions of CH_2OH and CH_3O (dissociation, isomerization, reaction with O_2). Table 1 lists the reactions in the methanol subset; in the following, the numbering of the reactions corresponds to the numbers in this table. The full reaction mechanism is available as Supplemental Material.

3.1 Ab initio calculations

In the present work, the rate constants for the CH_2OH/CH_3O dissociation / isomerization system and for the CH_3O+O_2 reaction have been calculated by ab initio methods. Because of the occurrence of significant spin-contamination, coupled-cluster approaches were employed. In brief, geometries and frequencies (scaled by 0.954) of reactants and transition states were derived with CCSD/6-311G(d,p) using the Gaussian 09 program [26], and are summarized in the Supplemental Material. For the reactions $CH_2OH \rightleftharpoons CH_2O+H$ (R11), $CH_3O \rightleftharpoons CH_2O+H$ (R19), and $CH_3O \rightleftharpoons CH_2OH$ (R20), energies were obtained with the Molpro09 program [27] at the CCSD(T)/aug-cc-pVnZ levels of theory with n=3-5, and extrapolated as exp(-n) to the infinite basis set limit. For the larger CH_3O+O_2

$\rightleftharpoons$ CH_2O+HO_2 (R27) system, energies were assessed via the CBS-QB3 method [28] which approximates this extrapolated limit. Table 2 lists the energies of the stationary points in the $C/H_3/O_3$ system derived with coupled cluster theory.

Previous studies of the four reactions considered here provided preliminary structures for the transition state (TS) optimizations [29, 30]. The thermochemistry of methoxy and hydroxymethyl radicals is complicated by significant anharmonicity, coupling between normal modes, spin-orbit splitting and Jahn-Teller distortion, which have been analyzed in some detail by Ruscic et al. [31]. For CH_3O we used the empirical electronic partition function based on splitting of the ^2E ground electronic state into $^2E_{3/2}$ and $^2E_{1/2}$ components, and a rotational symmetry number based on the average C_{3V} symmetry, although a Jahn-Teller-distorted C_s symmetry was used for the energy calculations. We found this model reproduced the tabulated thermochemistry [31] reasonably well: the error in entropy is -0.7 J K^{-1} mol^{-1} at 298 K increasing to -4.1 J K^{-1} mol^{-1} at 1200 K, while the error in H(T)-H(0 K) varies from 0.2 to 2.5 kJ mol^{-1} over this range of temperature. We treated CH_2OH as having a hindered OH rotor separable from the other modes which were treated as harmonic oscillators. This is certainly incorrect [31] and neglects anharmonicity and coupling of this rotor to the other motions. The impact of the seriously incorrect *ab initio* vibrations computed at 451 and 711 cm^{-1} instead of 234 and 420 cm^{-1} is, fortuitously, to compensate for the neglected coupling with the result that the computed entropy is too small by the amount of 3.7 J K^{-1} mol^{-1} decreasing to 1.5 J K^{-1} mol^{-1} over 298 – 1200 K, and H(T)-H(0 K) is underestimated by 0.5 kJ mol^{-1} at 298 K and overestimated by 1.1 kJ mol^{-1} at 1200 K. These are modest errors.

RRKM and transition state theories as implemented within the Multiwell program [32] were applied to derive kinetics over 600-1200 K and 0.01-100 bar (see Table 1). The Multiwell program allows for quantum mechanical tunneling estimated from an Eckart potential. For the RRKM calculations,

we assumed Lennard-Jones parameters of 417 K and 3.69 Å, taken from Chemkin, and an exponential down energy transfer model with $\alpha = 350$ cm^{-1}.

The potential energy diagram summarized in Fig. 1 indicates that unimolecular decomposition of CH_3O energetically favors CH_2O formation over isomerization to CH_2OH. In fact the isomerization also has a rather tight TS, with an A factor at 800 K and the high-pressure limit of 2.4×10^{13} s^{-1} vs 1.6×10^{14} s^{-1} for $k_{19,\infty}$. For this reason most unimolecular decomposition of CH_2OH yields CH_2O+H (A factor 7.8×10^{13} s^{-1}) rather than CH_3O (A factor 5.6×10^{12} s^{-1}), even though their energies are similar. Any CH_3O formed by isomerization of CH_2OH initially has sufficient excess energy to further react on to CH_2O+H. This means that isomerization is a minor channel and does not maintain equilibrium between the two CH_3O isomers.

Figure 2 shows an Arrhenius plot for the reactions $CH_2OH \rightleftharpoons CH_2O$+H (R11), $CH_3O \rightleftharpoons CH_2O$+H (R19), and $CH_3O \rightleftharpoons CH_2OH$ (R20). Of these steps, only the rate constant for $CH_3O \rightleftharpoons CH_2O$+H (R19) has been measured experimentally. Hippler et al. [33] derived a value for the high pressure limit of (R19) from experiments covering pressure and temperature ranges of 1–90 bar and 680–810 K. Their value for $k_{19,\infty}$ is about a factor of two lower than the one determined in the present work. Presently, we are not certain about the source of this discrepancy. It may partly be attributed to the fact that they neglected tunneling. According to our calculations, tunneling increases $k_{19,\infty}$ by 30-40% in the 600-800 K range, and it may also affect the falloff behavior.

For the CH_3O+O_2 reaction (R27), an Arrhenius plot is shown in Fig. 3. While the low-temperature data for this reaction are largely consistent, the behavior at elevated temperatures has been controversial. From experiments, Wantuck et al. [42] reported a nonlinear Arrhenius behavior, with

the rate constant increasing strongly above 600 K. However, their results have been questioned due to possible interference by thermal dissociation of CH_3O (R19) at the higher temperatures. For this reason, Baulch et al. [34] chose to disregard the data from Wantuck et al. in their evaluation of k_{19}. It is interesting to note that our theoretical rate constant (denoted by the solid line in Fig. 3) supports the observation of Wantuck et al. of a nonlinear Arrhenius behavior, even though the temperature dependence is smaller than in their determination. Our rate constant is in good agreement with the literature data, but significantly higher than the recommendation of Baulch et al. [34] at elevated temperatures (Fig. 3). This has some implications for the modeling in the present work.

3.2 Reaction mechanism

The methanol subset of the reaction mechanism is listed in Table 1. The main methanol consumption pathways under the present conditions are hydrogen abstraction reactions with H and OH. It is now well established that these steps mainly yield hydroxymethyl, while methoxy is only a minor product. For the CH_3OH+H reaction,

$CH_3OH+H \rightleftharpoons CH_2OH+H_2$ (R2)

$CH_3OH+H \rightleftharpoons CH_3O+H_2$ (R3)

the recent rate constants of Moses et al. [22] have been preferred, while for CH_3OH+OH,

$CH_3OH+OH \rightleftharpoons CH_2OH+H_2O$ (R6)

$CH_3OH+OH \rightleftharpoons CH_3O+H_2O$ (R7)

we use the values recommended by Rasmussen et al. [15]. The reactions of CH_3OH with HO_2,

$CH_3OH+HO_2 \rightleftharpoons CH_2OH+H_2O_2$ (R8)

$CH_3OH+HO_2 \rightleftharpoons CH_3O+ H_2O_2$ (R9)

and O_2,

$CH_3OH+O_2 \rightleftharpoons CH_2OH+HO_2$ (R10)

are important for ignition, but in the past kinetic models have had to rely on rough estimates for their rate constants. Two recent high-level theoretical studies offer rate constants for these steps with a strongly improved accuracy. For the CH_3OH+HO_2 reaction, we adopt the results of Alecu and Truhlar [24], while the rate constant for CH_3OH+O_2 is drawn from the work of Klippenstein et al. [23].

It is important to distinguish between CH_2OH and CH_3O, because the reactivity of these isomers is different. The CH_2OH isomer has a fairly high thermal stability and under fuel-lean conditions and not too high temperatures CH_2OH reacts preferably with O_2 to form HO_2,

$CH_2OH+O_2 \rightleftharpoons CH_2O+HO_2$ (R18)

The CH_3O isomer dissociates easily in a reaction that forms atomic hydrogen,

$CH_3O \rightleftharpoons CH_2O+H$ (R19)

Since the HO_2 radical is comparatively unreactive, the partitioning among CH_3O and CH_2OH is important for the methanol oxidation rate. While the values of k_{18} and k_{19} are well established, the rate constants for dissociation of the hydroxymethyl radical, $CH_2OH \rightleftharpoons CH_2O+H$ (R11), for the isomerization of methoxy to hydroxymethyl radical, $CH_3O \rightleftharpoons CH_2OH$ (R20), and for methoxy reacting with oxygen, $CH_3O+O_2 \rightleftharpoons CH_2O+HO_2$ (R27), have been in dispute in the past, as discussed above. We consider the rate coefficients derived in the present work for these steps to be more reliable than data in the literature and recommend that they are used in kinetic modeling.

4. Results and Discussion

Oxidation of methanol has been studied in a flow reactor in the temperature range 600-900 K and in the pressure interval 20-100 bar as a function of excess air ratio (λ=0.25-16). Table 3 lists the conditions of the experiments. They were conducted under dilute conditions with the balance made up of N_2. The constant flow of 5000 mL/min (STP) resulted in gas residence times in the isothermal zone being a function of the reaction temperature and pressure, $t_r(s)=65.85 \cdot P(bar)/T(K)$. The experimental results were analyzed in terms of the detailed chemical kinetic model described above. All model calculations were performed using SENKIN, the plug flow reactor code that runs in conjunction with the Chemkin-II library [43, 44].

Figures 4-6 compare experimental and predicted results for CH_3OH, CO and CO_2, obtained under reducing conditions (λ=0.25) as a function of temperature at pressures of 20, 50, and 100 bar, corresponding to sets 1-3 in Table 3. The scatter in the data for the methanol concentration below 700 K indicates that the liquid fuel feeding is not completely stable over time. However, the fluctuations are mostly within 10% of the nominal inlet concentration for CH_3OH.

The results show that increasing pressure tends to lower the onset temperature for methanol oxidation, which changes from about 775 K at 20 bar to 700 K at 100 bar. It should be noted that the shift observed in the figures is partly caused by the increase in residence time at higher pressure (Table 3), but increased pressure also promotes ignition. At the higher temperatures, the increase in pressure serves to inhibit slightly the consumption of CH_3OH. Methane and ethanol were also detected among the products at higher temperatures, but only in very small amounts. The modeling predictions are in satisfactory agreement with the experimental results, even though the CO concentrations are slighty overpredicted at the higher temperatures.

Figures 7 and 8 show results obtained at stoichiometric and oxidizing conditions, respectively, at 100 bar. Comparison of figures 6-8 shows that the temperature for onset of reaction, approximately 700 K, is almost independent of stoichiometry. As would be expected, the oxygen concentration has a pronounced effect on the consumption of CH_3OH and formation of CO and CO_2. While for fuel-rich conditions (λ=0.25), the exit CO concentration increases gradually with temperature, it reaches a peak value at around 750 K for stoichiometric (λ=1.0) and fuel-lean (λ=16) conditions. At this temperature, the methanol has been fully consumed and no longer competes for OH radicals. As the temperature increases further, the CO_2 concentration would be expected to increase as well due to the oxidation of CO to CO_2. However, it is noteworthy that even under very lean conditions (Fig. 8), as much as 800 ppm of CO is found in the exit stream from the reactor. The model captures the effect of stoichiometry well and also predicts the fairly high CO level observed even at lean conditions. Actually, according to the model there is a small local minimum in CO at about 800 K under both stoichiometric and lean conditions (Figs. 7 and 8), but this cannot be confirmed from the experimental results.

The main reaction routes for methanol oxidation under the present conditions are shown in Fig. 9. Methanol is consumed by reaction with OH (R6/R7) and, under fuel-rich conditions, H (R2). These reactions yield hydroxymethyl and methoxy radicals, with the former radical being predominant. As expected [13-15], the hydroxymethyl radical mainly react with oxygen (R18), while methoxy undergoes thermal decomposition (R19). However, due to the larger value of k_{27} in the present work, compared to previous modeling studies, the reaction of CH_3O with O_2 (R27) becomes competitive under lean conditions. Finally, formaldehyde formed in these reactions is converted to CO and CO_2 through the sequence $CH_2O \rightarrow HCO \rightarrow CO \rightarrow CO_2$. Some CO_2 is also produced directly from the formyl radical by the reaction with HO_2 under fuel-rich conditions at 20 bar, and from CO, with HOCO as an intermediate species, under stoichiometric and fuel-lean conditions. The main reaction

pathways under the present conditions are consistent with those reported for atmospheric pressure [13-15]. Unlike unsaturated fuels such as ethylene [45], the high pressure does not introduce additional oxidation pathways for methanol because addition reactions of OH and O_2 are not important.

A first order sensitivity analysis shows that the predicted onset temperature is sensitive to the same subset of reactions, independent of stoichiometry. The highest positive sensitivity coefficients are found for the important initiation steps,

$CH_3OH+HO_2 \rightleftharpoons CH_2OH+H_2O_2$ (R8)

$H_2O_2(+M) \rightleftharpoons OH+OH(+M)$

while initiation is inhibited by the terminating reaction

$HO_2+HO_2 \rightleftharpoons H_2O_2+ O_2$

Also the reactions of CH_3OH with OH (R6, R7) and O_2 (R10), as well as $CH_2O + HO_2$, show up in the sensitivity analysis.

To test if the present mechanism can predict the autoignition behavior of methanol/oxidizer mixtures at high pressures and moderate temperatures, we used it to simulate the autoignition delay times measured in a RCM by Kumar et al. [16]. For a meaningful comparison between measurements and simulations one must account for deviations from ideal behavior that occur during the experiments, such as heat loss, and it is necessary to take into account the entire compression history of the gas mixture in the simulations. Towards this end the specific volume of the assumed adiabatic core is used as input parameter in the simulations. Similar to the procedure described by Gersen and coworkers [46, 47], we determined the specific volume from the measured pressure in the period between compression and the moment after compression where substantial heat release begins (~1

ms prior the minimum in the pressure trace after compression), and extrapolate the time dependence in this fashion to the region in which substantial heat release begins. The entire derived history of the specific volume is used as input into the simulations. Again, the simulations are performed with the SENKIN code [43].

Figure 10 shows two pressure traces measured by Kumar et al. [16] in a stoichiometric $CH_3OH/O_2/Ar$ mixture at different compressed peak pressures of P_c~15 bar (thin solid line) and P_c~30 bar (bold solid line) and compressed peak temperature conditions of T_c~916 K and T_c~ 904 K, respectively. Comparison of the measured and simulated pressure profiles (Fig. 10) shows that the ignition delay times are underpredicted at stoichiometric conditions; for the P_c~30 bar case the difference is about 25% and at P_c~15 bar the difference between the calculated and measured autoignition delay time is about ~40%. Figure 11 presents the measured and calculated ignition delay times of $CH_3OH/O_2/Ar$ mixtures at P_c~15 bar and at an equivalence ratio of φ=0.25 as function of the reciprocal temperature. As can be seen from Fig. 11, the calculations for the lean conditions are in good agreement with the measurements over the entire measured domain.

5. Conclusions

The methanol oxidation has been studied in a flow reactor in the temperature range 600-900 K and in the pressure interval 20-100 bar as a function of stoichiometry. While the temperature for onset of reaction is largely independent of stoichiometry, it decreases significantly with increasing pressure. The experimental results from the present work, as well as RCM ignition delays reported in literature, have been compared with an updated chemical kinetic model. Ab initio calculations and RRKM analysis were used to obtain rate coefficients for key reactions of CH_2OH and CH_3O (dissociation, isomerization, reaction with O_2). Modeling predictions were generally in good

agreement with the experimental results. Rate-of-production analysis and sensitivity analysis were used to identify the important reactions. The predicted onset of reaction was particularly sensitive to the reaction $CH_3OH+HO_2 \rightleftharpoons CH_2OH+H_2O_2$.

Acknowledgments

The work is part of the CHEC (Combustion and Harmful Emission Control) research program. It was financially supported by the Technical University of Denmark and the Danish Technical Research Council. The authors would also like to express their gratitude to Ministerio de Ciencia e Innovación (MICINN) through project CTQ2009-12205, for financial support. Ms. V. Aranda acknowledges the MICINN for the pre-doctoral grant awarded. PM thanks the R.A. Welch Foundation (Grant B-1174) for support. The computational facilities were purchased in part with NSF grant CHE-0741936. The authors would also like to thank S.J. Klippenstein for fruitful discussions.

References

[1] Ribeiro, N.M.; Pinto, A.C.; Quintella, C.M.; da Rocha, G.O.; Teixeira, L.S.G.; Guarieiro, L.L.N.; do Carmo Rangel, M.; Veloso, M.C.C.; Rezende, M.J.C.; Serpa da Cruz, R.; de Oliveira, A.M.; Torres, E.A.; de Andrade, J.B. Energy Fuels 2007, 21, 2433-2445.

[2] Chao, M.R.; Lin, T.C.; Chao, H.R.; Chang, F.H.; Chen, C.B. Sci. Total Environ. 2001, 279, 167-179.

[3] Sayin, C.; Ilhan, M.; Canakci, M.; Gumus, M. Renewable Energy 2009, 34, 1261-1269.

[4] Canakci, M.; Sayin, C.; Gumus, M. Energy Fuels 2008, 22, 3709-3723.

[5] Yao, C.; Cheung, C.S.; Cheng, C.; Wang, Y.; Chan, T.L.; Lee, S.C. Energy Convers. Manage. 2008, 49, 1696-1704.

[6] Egolfopoulos, F.N.; Du, D.X.; Law, C.K. Combust. Sci. Technol. 1992, 83, 33-75.

[7] Li, S.C.; Williams, F.A. Proc. Combust. Inst. 1996, 26, 1017-1024.

[8] Liao, S.Y., Jiang, D.M.; Huang, Z.H.; Zeng, K. Fuel 2006, 85, 1346-1353.

[9] Dayma, G.; Ali, K.H. Dagaut, P. Proc. Combust. Inst. 2007, 31, 411-418.

[10] Bell, K.M.; Tipper, C.F.H. Trans. Faraday Soc. 1957, 53, 982-990.

[11] Aniolek, K.W.; Wilk, R.D. Energy Fuels 1995, 9, 395-405.

[12] Norton, T.S.; Dryer, F.L. Combust. Sci. Technol. 1989, 63, 107-129.

[13] Held, T.J.; Dryer, F.L. Int. J. Chem. Kinet. 1998, 30, 805-830.

[14] Alzueta, M.U.; Bilbao, R.; Finestra, M. Energy Fuels 2001, 15, 724-729.

[15] Rasmussen, C.L.; Wassard, K.H.; Dam-Johansen, K.; Glarborg, P. Int. J. Chem. Kinet. 2008, 40, 423-441.

[16] Kumar, K.; Sung, C.J. Int. J. Chem. Kinet. 2011, 43, 175-184.

[17] Cribb, P.H.; Dove, J.-E.; Yamazaki, S. Combust. Flame 1992, 88, 186-200.

[18] Rasmussen, C.L.; Hansen, J.; Marshall, P.; Glarborg, P. Int. J. Chem. Kinet. 2008, 40, 454-480.

[19] Christensen, J.M.; Jensen, P.A.; Jensen, A.D. Ind. Eng. Chem. Res. 2011, 50, 7949-7963.

[20] Rasmussen, C.L.; Jakobsen, J.G.; Glarborg, P. Int. J. Chem. Kinet. 2008, 40, 778-807.

[21] Rasmussen, C.L.; Rasmussen, A.E.; Glarborg, P. Combust. Flame 2008, 154, 529-545.

[22] Moses, J.I.; Visscher, C.; Fortney, J.J.; Showman, A.P.; Lewis, N.K.; Griffith, C.A.; Klippenstein, S.J.; Shabram, M.; Friedson, A.J.; Marley, M.S.; Freedman, R.S. Astrophys. J. 2011, 737, 15.

[23] Klippenstein, S.J.; Harding, L.B.; Davis, M.J.; Tomlin, A.S.; Skodje, R.T. Proc. Combust. Inst. 2011, 33, 351-357.

[24] Alecu, I.M.; Truhlar, D.G. J. Phys. Chem. A 2011, 115, 14599-14611.

[25] Mousavipour, S.H.; Homayoon, Z. J. Phys. Chem. A 2011, 115, 3291-3300.

[26] Frisch, M.J.; et al., Gaussian 09 rev B.01, Gaussian: Wallingford, CT, (2009)

[27] Werner, H.J.; et al., Molpro09 (2009)

[28] Montgomery, J.A.; Frisch, M.J.; Ochterski, J.W.; Petersson, G.A. J. Chem. Phys. 1999, 110, 2822-2827

[29] Saebø, S.; Radom, L.; Schaefer, H.F. III. J. Chem. Phys. 1983, 78, 845-853.

[30] Bofill, J.M.; Olivella, S.; Solé, A.; Anglada, J.M. J. Am. Chem. Soc. 1999, 121, 1337-1347.

[31] Ruscic, B.; Boggs, J.E.; Burcat, A.; Császár, A.G.; Demaison, J.; Janoschek, R.; Martin, J.M.L.; Morton, M.L.; Rossi, M.J.; Stanton, J.F.; Szalay, P.G.; Westmoreland, P.R.; Zabel, F.; Bérces, T. J. Phys. Chem. Ref. Data 2005, 34, 573-656.

[32] Barker, J.R. Int. J. Chem. Kinet. 2001, 33, 232-245 and MultiWell-2011.1, designed and maintained by John R. Barker with contributors Nicholas F. Ortiz, Jack M. Preses, Lawrence L. Lohr, Andrea Maranzana, Philip J. Stimac, T. Lam Nguyen, and T. J. Dhilip Kumar; University of Michigan, Ann Arbor, MI; http://aoss.engin.umich.edu/multiwell (2011)

[33] Hippler, H.; Striebel, F.; Viskolcz, B. Phys. Chem. Chem. Phys. 2001, 3, 2450-2458.

[34] Baulch, D.L., Bowman, C.T., Cobos, C.J., Cox, R.A., Just, T., Kerr, J.A., Pilling, M.J., Stocker, D., Troe, J., Tsang, W., Walker, R.W., Warnatz, J. J. Phys. Chem. Ref. Data 2005, 34, 757-1397.

[35] Wiebe, H.; Villa, A.; Hellman, T.M.; Heiklen, J. J. Am. Chem. Soc. 1973, 95, 7..

[36] Alcock, W.G.; Mile, B. Combust. Flame 1975, 24, 125.

[37] Barker, J.R.; Benson, S.W.; Golden, D. Int. J. Chem. Kinet. 1977, 9, 31.

[38] Kirsch, L.J.; Parkes, D.A. J. Chem. Soc. Faraday Trans. 1, 1981, 77, 293.

[39] Batt, L.; Robinson, G.N. Int. J. Kinetic. 1979, 11, 1045.

[40] Cox, R.A.; Derwent, R.G.; Kearsey, S.V.; Batt, L.; Patrick, K.G. J. Photochem. 1980, 13, 149.

[41] Bofill, J.M.; Olivella, S.; Sole, A.; Anglada, J.M. J. Am. Chem. Soc. 1999, 121, 1337.

[42] Wantuck, P.J.; Oldenborg, R.C.; Baughcum, S.L.; Winn, K.R. J. Chem. Phys. 1987, 91, 4653–4655.

[43] A.E. Lutz, R.J. Kee, J.A. Miller, SENKIN: a Fortran program for predicting homogeneous gas phase chemical kinetics with sensitivity analysis. Sandia Report SAND87-8248. Sandia National Laboratories (1988).

[44] R.J. Kee, F.M. Rupley, J.A. Miller, CHEMKIN II: A fortran chemical kinetics package for the analysis of gas phase chemical kinetics. Sandia Report SAND87-8215. Sandia National Laboratories (1991).

[45] Lopez, J.G.; Rasmussen, C.L.; Alzueta, M.U.; Gao, Y.; Marshall, P.; Glarborg, P. Proc. Combust. Inst. 2009, 32, 367-375.

[46] Gersen, S.; Anikin, N.B. Mokhov, A.V.; Levinsky, H.B. Int. J. Hydrogen Energy 2008, 33, 1957-1964.

[47] Gersen, S.; Mokhov, A.V.; Darmeveil, J.H.; Levinsky, H.B.; Glarborg, P. Proc.Combust. Inst. 2011, 33, 433-440.

Table 1. Selected reactions in the methanol oxidation subset.

	A (cm^3/mol·s)	β	E_a(cal/mol)	Source
1. $CH_3OH(+M) \rightleftharpoons CH_3+OH(+M)$	2.1E18	-0.60	92540	[21]
Low-pressure limit:	2.6E49	-8.80	101500	
Troe parameters: 0.7656 1910 59.51 9374				
2. $CH_3OH+H \rightleftharpoons CH_2OH+H_2$	6.6E04	2.73	4449	[22]
3. $CH_3OH+H \rightleftharpoons CH_3O+H_2$	4.1E04	2.66	9221	[22]
4. $CH_3OH+O \rightleftharpoons CH_2OH+OH$	2.1E13	0.00	5305	[21]
5. $CH_3OH+O \rightleftharpoons CH_3O+OH$	3.7E12	0.00	5305	[21]
6. $CH_3OH+OH \rightleftharpoons CH_2OH+H_2O$	1.5E08	1.44	113	[21]
7. $CH_3OH+OH \rightleftharpoons CH_3O+H_2O$	2.7E07	1.44	113	[21]
8. $CH_3OH+HO_2 \rightleftharpoons CH_2OH+H_2O_2$	3.5E-04	4.85	10346	[24]
9. $CH_3OH+HO_2 \rightleftharpoons CH_3O+H_2O_2$	1.5E-03	4.61	15928	[24]
10. $CH_3OH+O_2 \rightleftharpoons CH_2OH+HO_2$	3.6E05	2.27	42760	[23]
11. $CH_2OH \rightleftharpoons CH_2O+H$	3.3E32	-7.18	39740	pw, 0.01 bar
	8.3E41	-9.58	45730	pw, 0.1 bar
	2.3E36	-7.53	44880	pw, 1 bar
	5.7E34	-6.64	46430	pw, 20 bar
	3.4E31	-5.57	45610	pw, 50 bar
	1.7E27	-4.21	44130	pw, 100 bar
	4.2E07	1.86	36590	pw, k_∞
12. $CH_2OH+H \rightleftharpoons CH_2O+H_2$	1.4E13	0.00	0	[21]
13. $CH_2OH+H \rightleftharpoons CH_3+OH$	6.0E12	0.00	0	[21]
14. $CH_2OH+H(+M) \rightleftharpoons CH_3OH(+M)$	4.3E15	-0.80	0	[21]
Low pressure limit:	3.8E37	-6.20	1333	
Troe parameters: 0.2500 210 1434 1.0E30				
15. $CH_2OH+O \rightleftharpoons CH_2O+OH$	6.6E13	0.00	-693	[21]
16. $CH_2OH+OH \rightleftharpoons CH_2O+H_2O$	2.4E13	0.00	0	[21]
17. $CH_2OH+HO_2 \rightleftharpoons CH_2O+H_2O_2$	1.2E13	0.00	0	[21]
18. $CH_2OH+O_2 \rightleftharpoons CH_2O+HO_2$	7.2E13	0.00	3736	[21]
Duplicate	2.9E16	-1.50	0	[21]
19. $CH_3O \rightleftharpoons CH_2O+H$	1.8E31	-6.96	26670	pw, 0.01 bar
	2.9E20	-3.64	20140	pw, 0.1 bar
	7.7E115	-32.10	63410	pw, 1 bar
	5.4E111	-30.46	62690	pw, 20 bar
	5.6E87	-23.06	52090	pw, 50 bar
	4.7E93	-24.61	57200	pw, 100 bar
	1.1E10	1.23	24250	pw, k_∞
20. $CH_3O \rightleftharpoons CH_2OH$	1.4E27	-5.99	27390	pw, 0.01 bar
	2.3E16	-2.66	20860	pw, 0.1 bar
	6.0E111	-31.12	64130	pw, 1 bar
	4.2E107	-29.49	63410	pw, 20 bar
	4.4E83	-22.09	53620	pw, 50 bar
	3.6E89	-23.64	57920	pw, 100 bar
	8.9E05	2.21	24970	pw, k_∞
21. $CH_3O+H \rightleftharpoons CH_2O+H_2$	5.3E13	0.00	745	[21]
22. $CH_3O+H \rightleftharpoons CH_3+OH$	4.6E12	0.00	745	[21]
23. $CH_3O+H(+M) \rightleftharpoons CH_3OH(+M)$	2.4E12	0.50	50	[21]

Low pressure limit: Troe parameters: 0.7000 100 90000 10000	4.7E40	-7.44	140803	
24. $CH_3O+O \rightleftharpoons CH_2O+OH$	3.8E12	0.00	0	[21]
25. $CH_3O+OH \rightleftharpoons CH_2O+H_2O$	1.8E13	0.00	0	[21]
26. $CH_3O+HO_2 \rightleftharpoons CH_3OH+O_2$	1.4E11	0.00	0	[25]
27. $CH_3O+O_2 \rightleftharpoons CH_2O+HO_2$	4.8E-01	3.57	-1055	pw

pw: present work

Table 2. Energies of stationary points in the $C/H_3/O_3$ system derived with coupled cluster theory.

Species	aug-cc-pVTZ	aug-cc-pVQZ	aug-cc-pV5Z	CBS limit	relative enthalpy at 0 K kJ/mol (a)
	Au	aug-cc-pVQZ	aug-cc-pV5Z	au	
CH_3O	-114.8850816	-114.9138885	-114.922965	-114.9271403	0
H	-0.49982118	-0.49994832	-0.49999478	-0.500021534	
CH_2O	-114.3428434	-114.3723302	-114.3815812	-114.3858104	82.4
CH_2OH	-114.8987541	-114.9286887	-114.9379937	-114.9421907	-37.6
TS-1, $CH_3O \rightarrow CH_2O+H$	-114.8367789	-114.8663888	-114.8756417	-114.8798475	103.0
TS-2,$CH_3O \rightarrow CH_2OH$	-114.8330452	-114.8622654	-114.8714234	-114.8756039	124.0
TS-3,$CH_2OH \rightarrow CH_2O+H$	-114.8269853	-114.8566007	-114.8658411	-114.8700318	127.0
O_2	-150.1407415	-150.1785442	-150.1909034	-150.1969069	
HO_2	-150.7265278	-150.7653707	-150.7780254	-150.7841404	-119.8

(a) Includes zero-point energy at CCSD/6-311G(d,p) level scaled by 0.954.

(b) The TS for $CH_3O + O_2 \rightarrow CH_2O + HO_2$ has an enthalpy of 13.1 kJ mol^{-1} relative to reactants based on CBS-QB3 energies obtained with CCSD/6-311G(d,p) geometries and zero-poin energies.

Table 3. Matrix of experimental conditions. The experiments are conducted at constant mass flow, 5000 ml(STP)/min, in the temperature range 600-900 K and pressure interval 20-100 bar. The residence time is dependent on the reaction temperature and pressure.

Exp	Pressure (bar)	CH_3OH (ppm)	O_2 (ppm)	NO_x (ppm)	λ	t_{res} (s)
Set 1	20	2606	904	0	0.23	1317/T
Set 2	50	2390	939	0	0.26	3293/T
Set 3	100	2370	951	0	0.27	6587/T
Set 4	100	3010	4500	0	1.00	6587/T
Set 5	100	2930	71300	0	16.2	6587/T

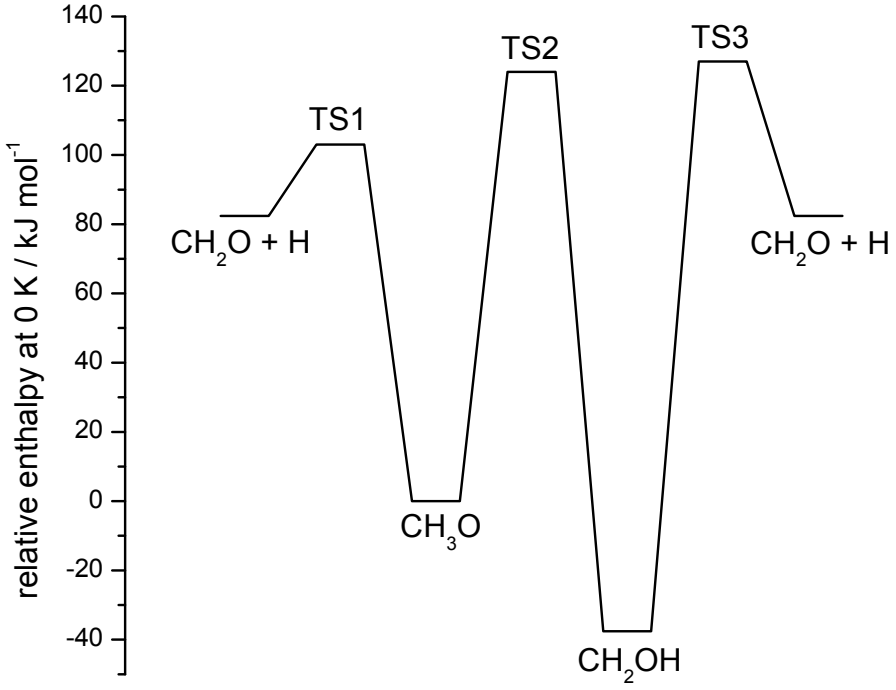

Figure 1. Relative enthalpies computed for 0 K based on CCSD(T) energies extrapolated to the complete basis set limit for the CH_3O/CH_2OH system.

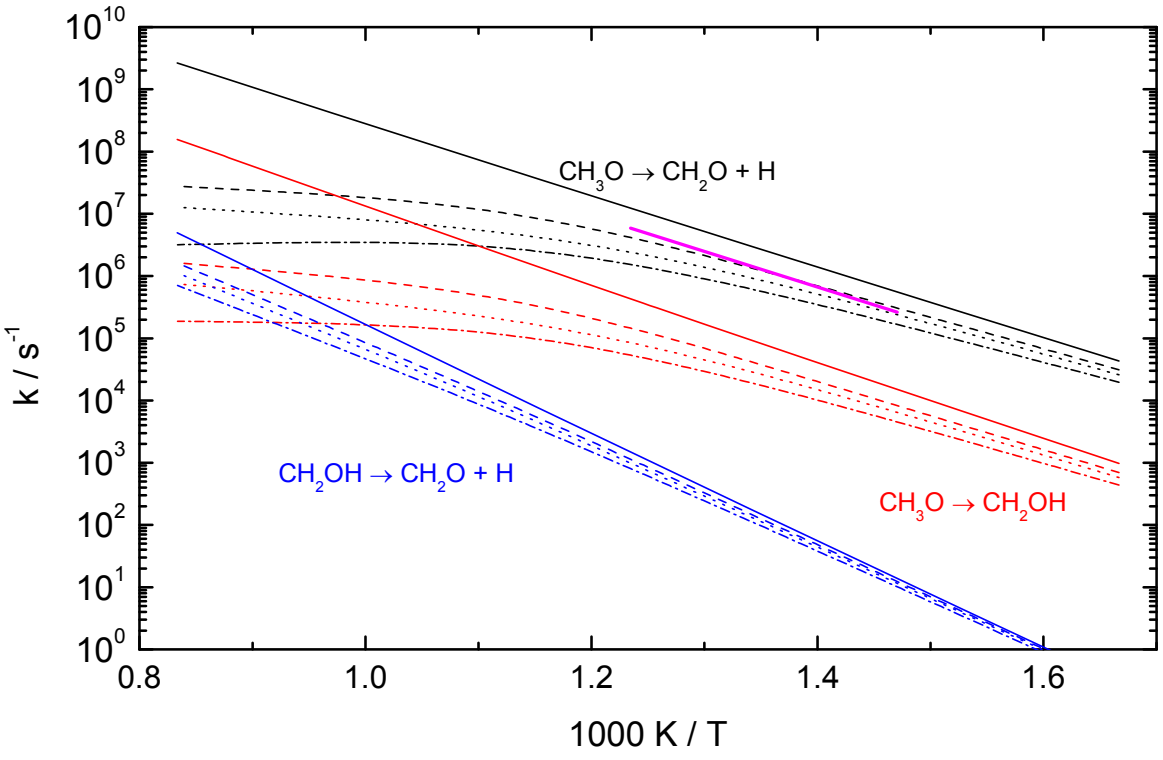

Figure 2. Arrhenius plot for the reactions $CH_2OH \rightleftharpoons CH_2O+H$ (R11), $CH_3O \rightleftharpoons CH_2O+H$ (R19), and $CH_3O \rightleftharpoons CH_2OH$ (R20) (lower). The (thin) solid lines denote the calculated high-pressure limit for each reaction, while pressure-specific rate constants are shown as dash-dotted lines (20 bar), short-dashed lines (50 bar), and long-dashed lines (100 bar). The thick solid line denotes the high-pressure limit derived by Hippler et al. [32] for (R19).

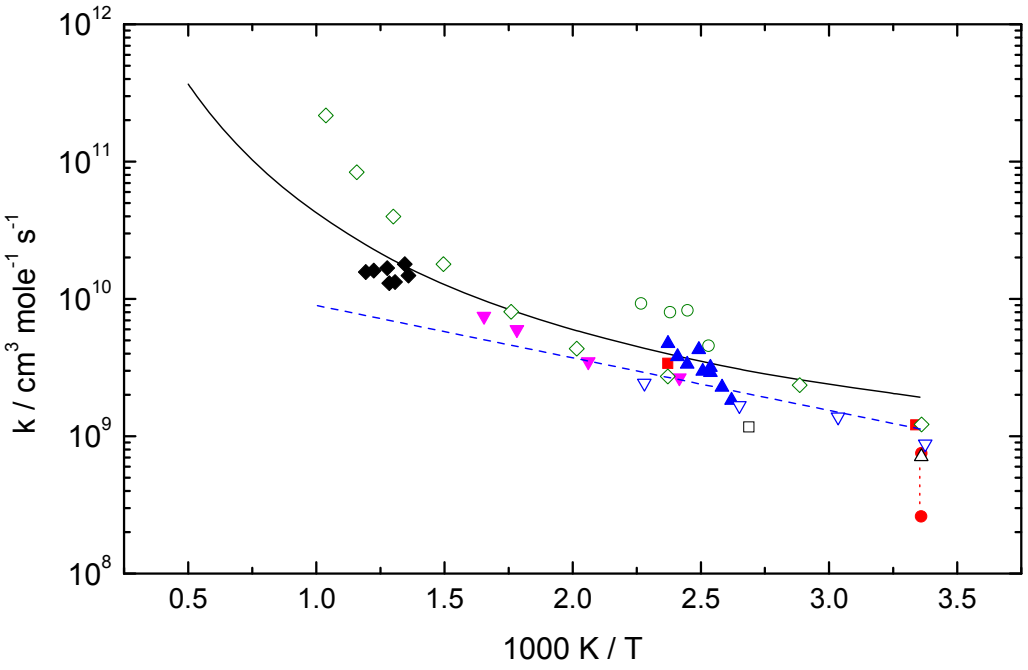

Figure 3. Arrhenius plot for the reaction $CH_3O+O_2 \rightleftharpoons CH_2O+HO_2$ (R27). Solid line: present work. Literature data: dashed line: CEC recommendation [33]; ● Wiebe et al. [34], □ Alcock and Mile [35], ○ Barker et al. [36], ■ Kirsch and Parkes [37],▲ Batt and Robinson [38], △ Cox et al. [39], ▼ Gutman et al., [40], ▽ Lorentz et al. [41], ♦ Zaslonko et al. [42], ◊ Wantuck et al. [43].

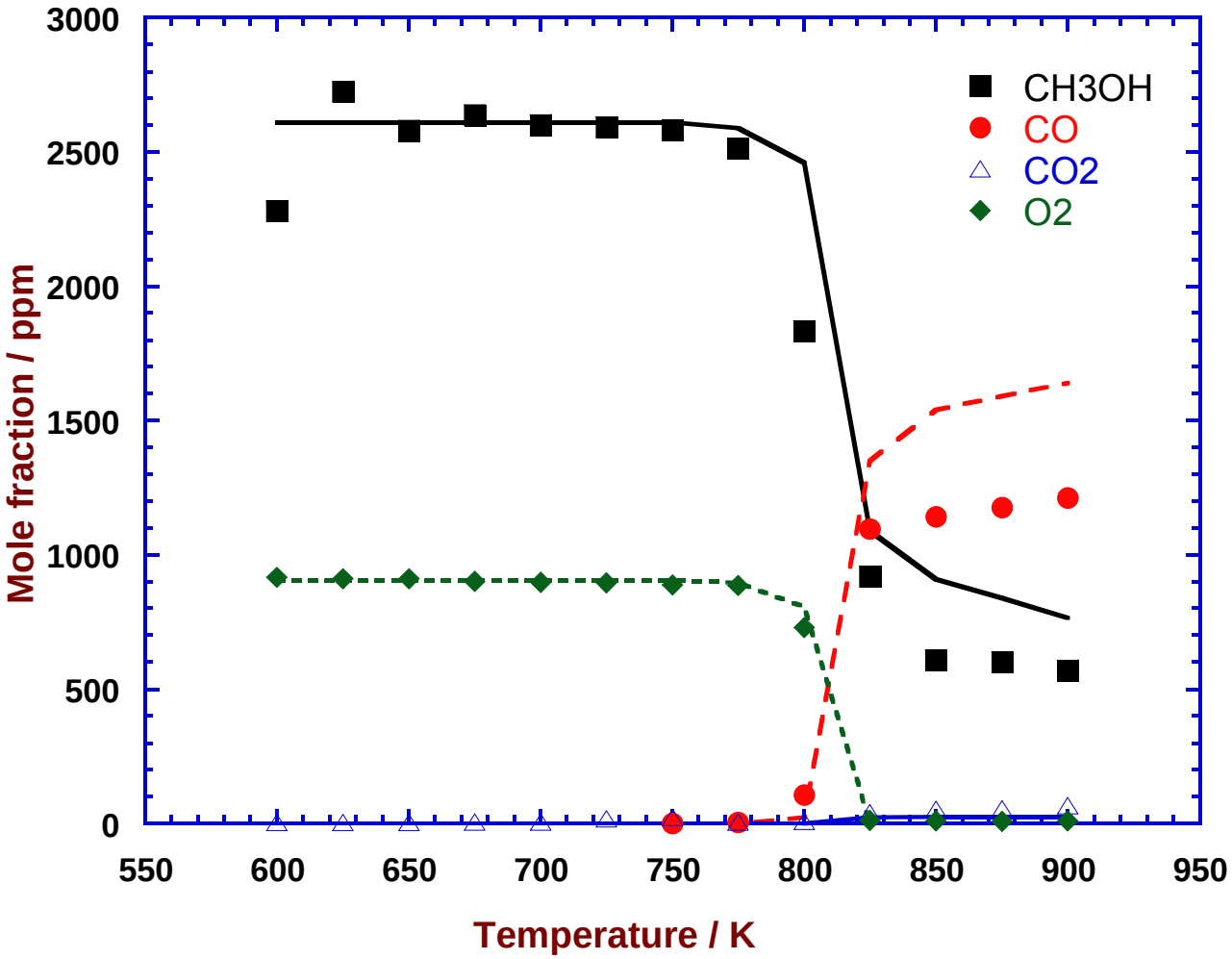

Figure 4. CH_3OH, CO, CO_2, and O_2 concentration profiles as a function of temperature for the conditions of set 1 in Table I (fuel-rich, 20 bar). Comparison between experimental data (symbols) and model predictions (lines).

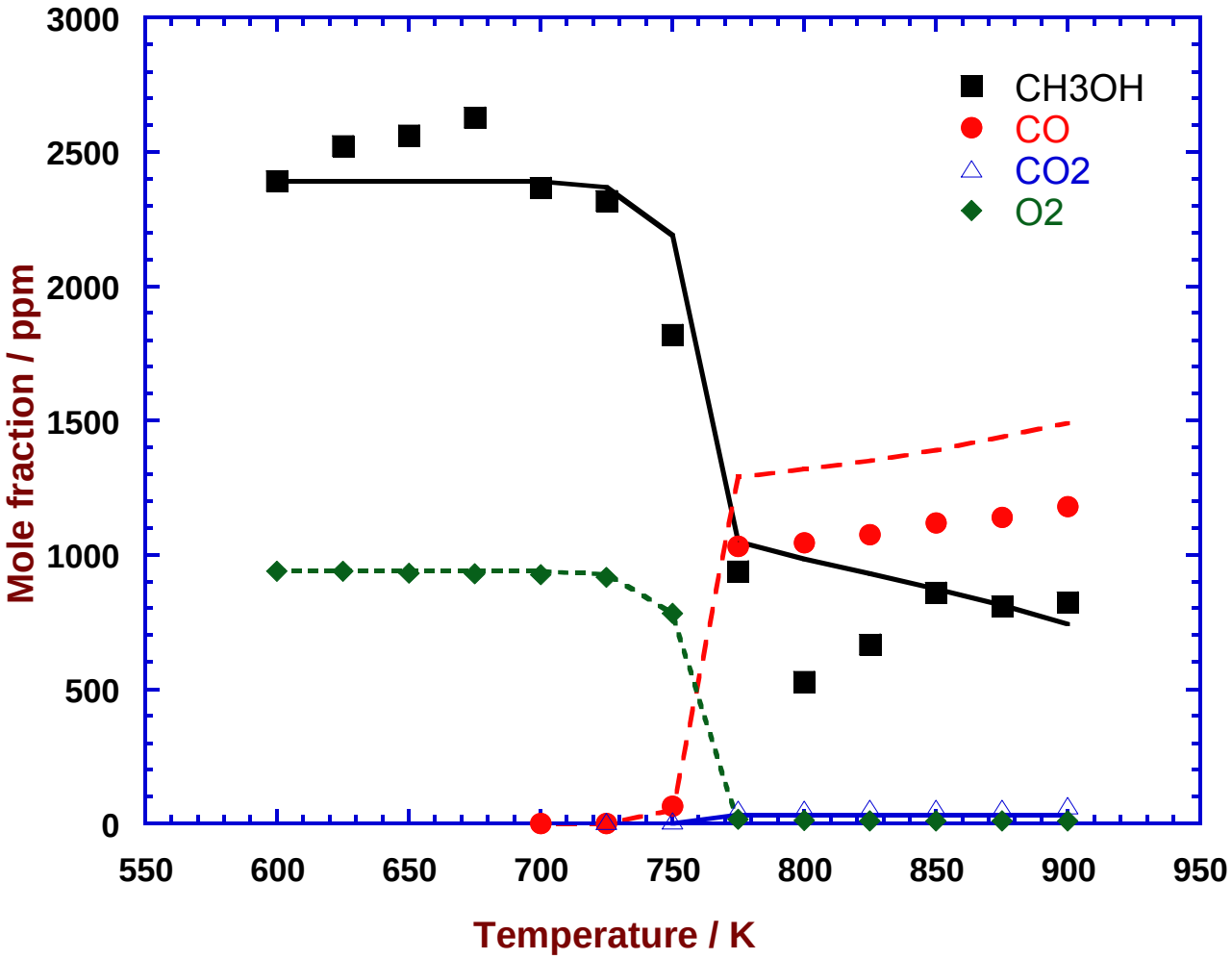

Figure 5. CH_3OH, CO, CO_2, and O_2 concentration profiles as a function of temperature for the conditions of set 2 in Table I (fuel-rich, 50 bar). Comparison between experimental data (symbols) and model predictions (lines).

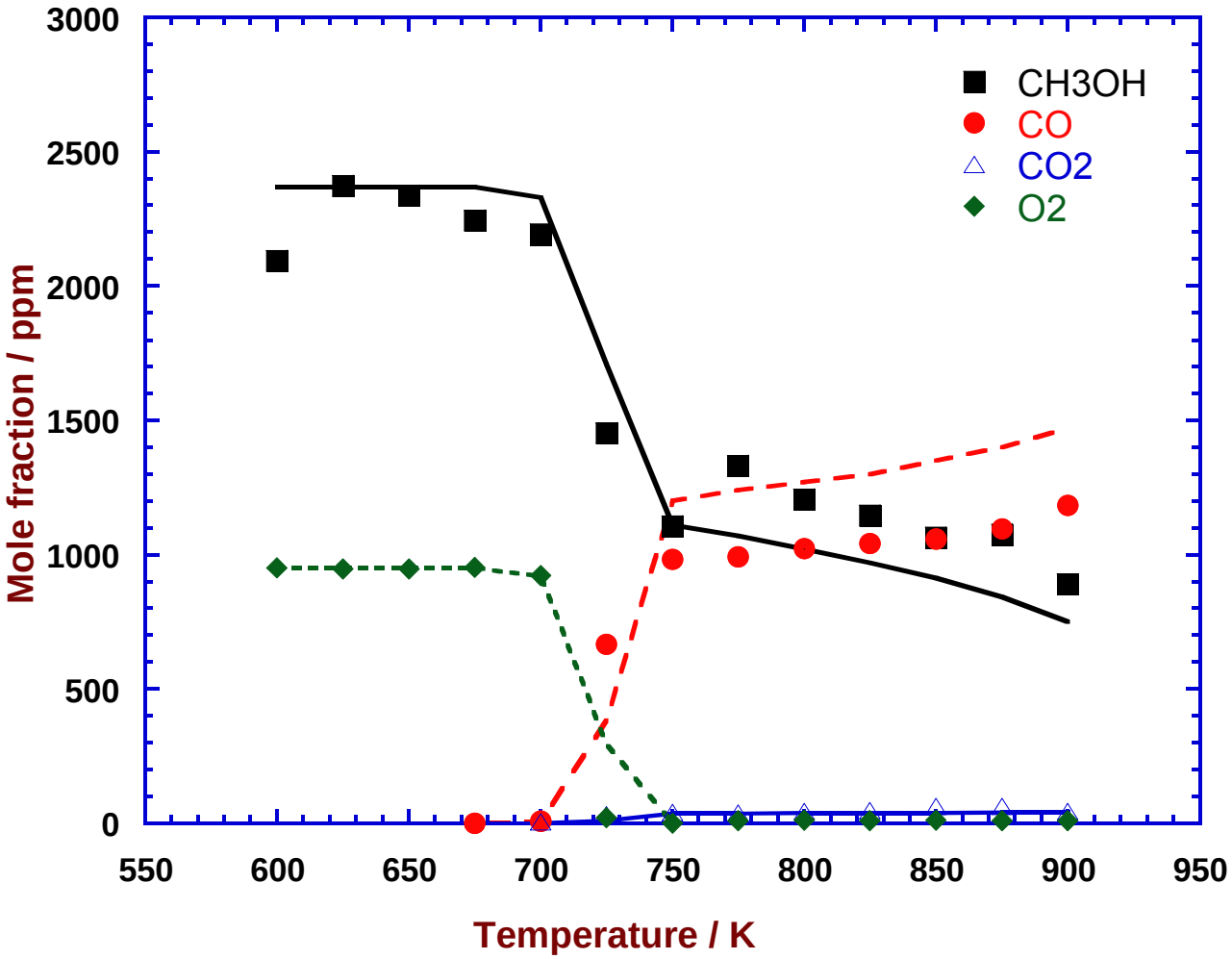

Figure 6: CH_3OH, CO, CO_2, and O_2 concentration profiles as a function of temperature for the conditions of set 3 in Table 3 (fuel-rich, 100 bar). Comparison between experimental data (symbols) and model predictions (lines).

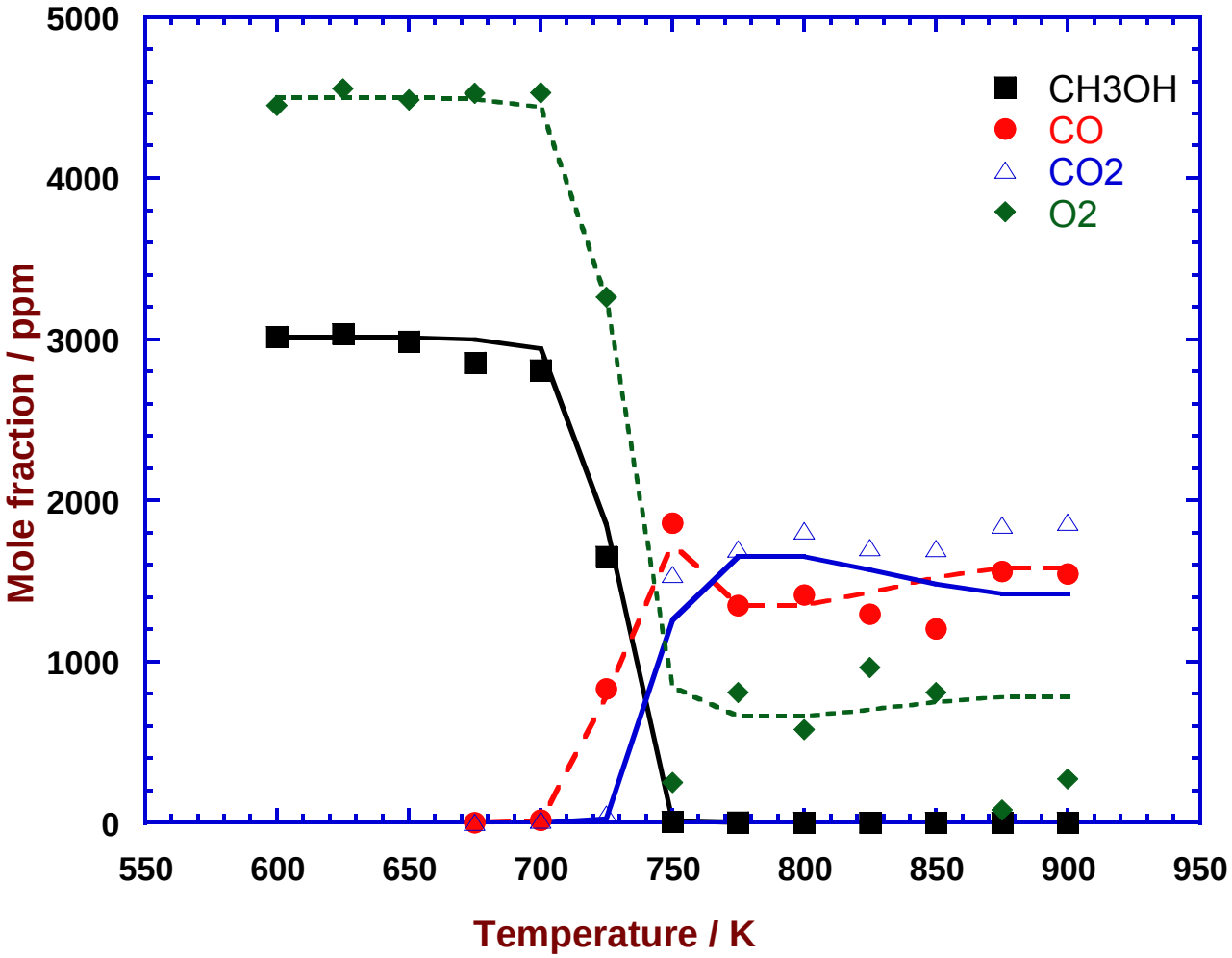

Figure 7: CH_3OH, CO, CO_2, and O_2 concentration profiles as a function of temperature for the conditions of set 4 in Table 3 (stoichiometric, 100 bar). Comparison between experimental data (symbols) and model predictions (lines).

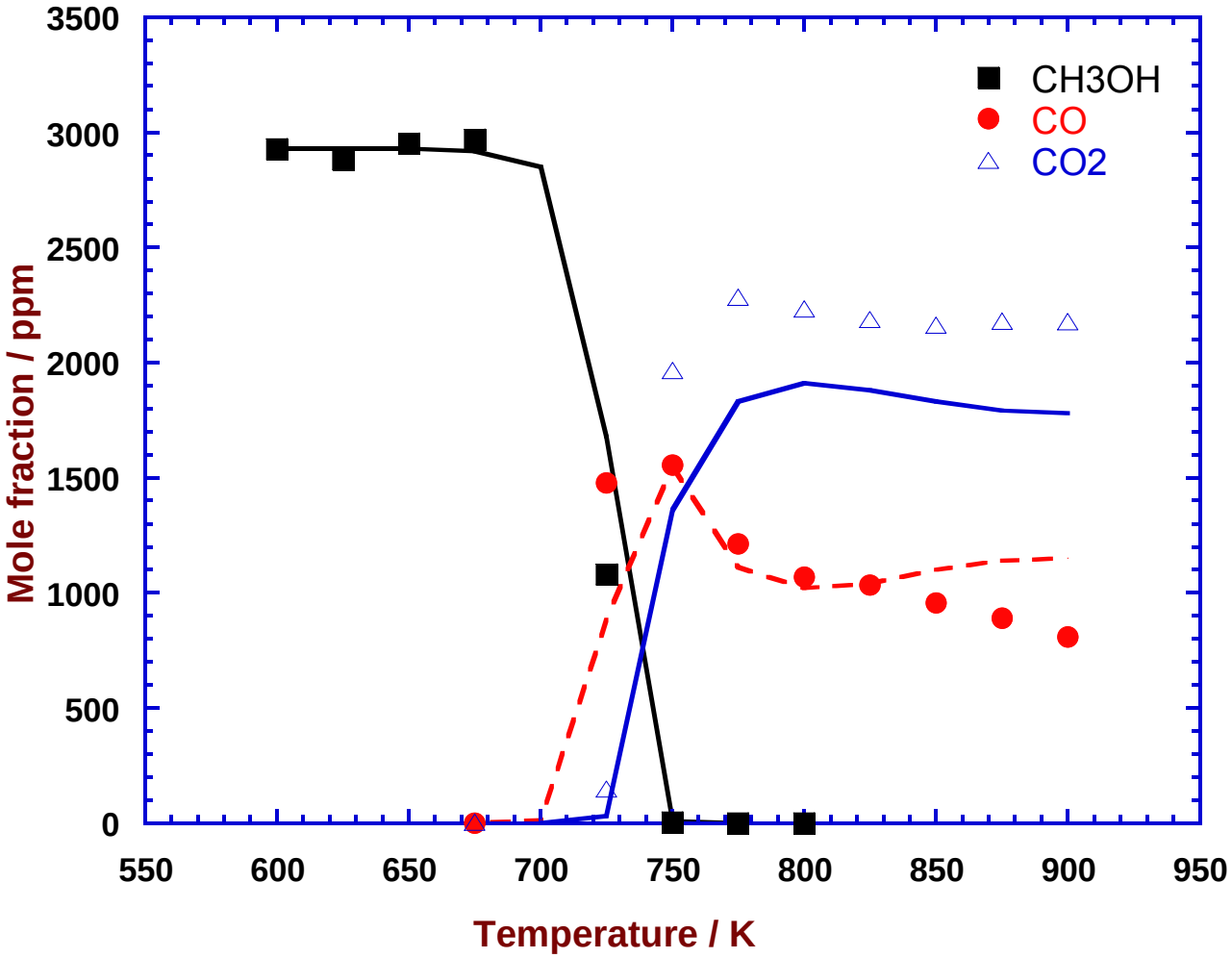

Figure 8: CH_3OH, CO, and CO_2 concentration profiles as a function of temperature for the conditions of set 5 in Table 3 (lean, 100 bar). Comparison between experimental data (symbols) and model predictions (lines).

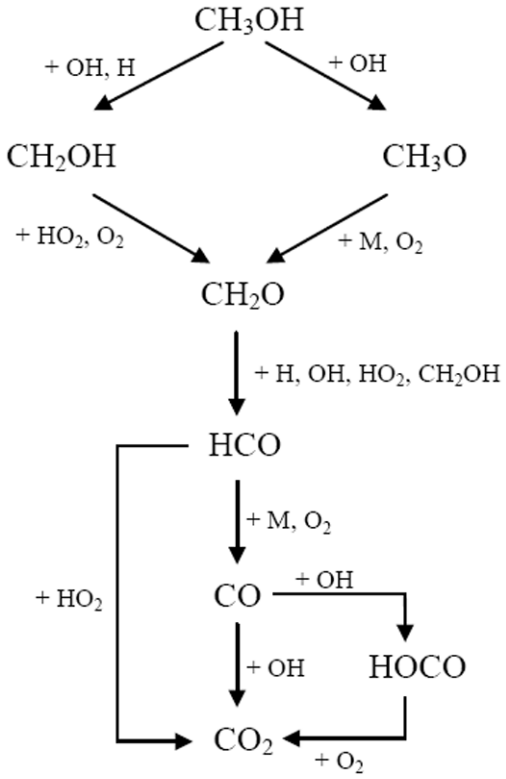

Figure 9. Reaction path diagram for methanol oxidation at the high pressure conditions of the present work.

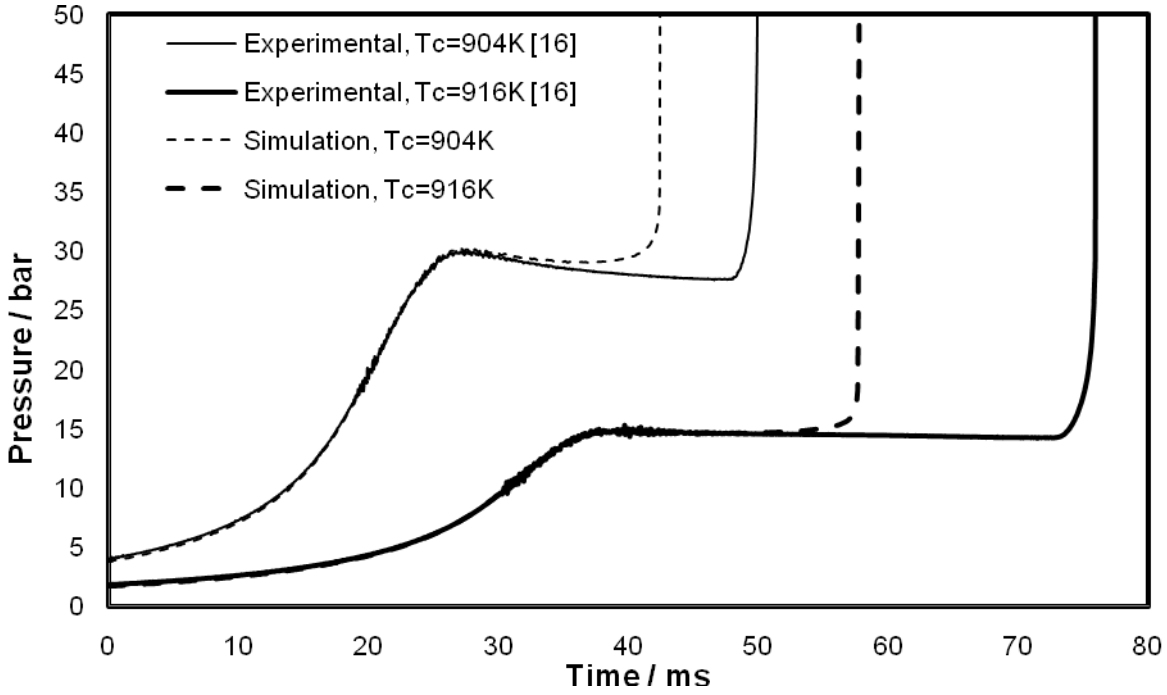

Figure 10. Measured and modeled pressure traces for stoichiometric methanol/O_2/Ar mixtures with O_2:Ar=1:3.76 at compressed peak pressures of P_c~15 bar (thin lines) and P_c~30 bar (solid lines) and compressed peak temperature conditions of T_c~916 K and T_c~ 904 K, respectively. The solid lines represent the measurements performed by Kumar et al. [16], and the dashed lines represent the simulations performed with the present mechanism.

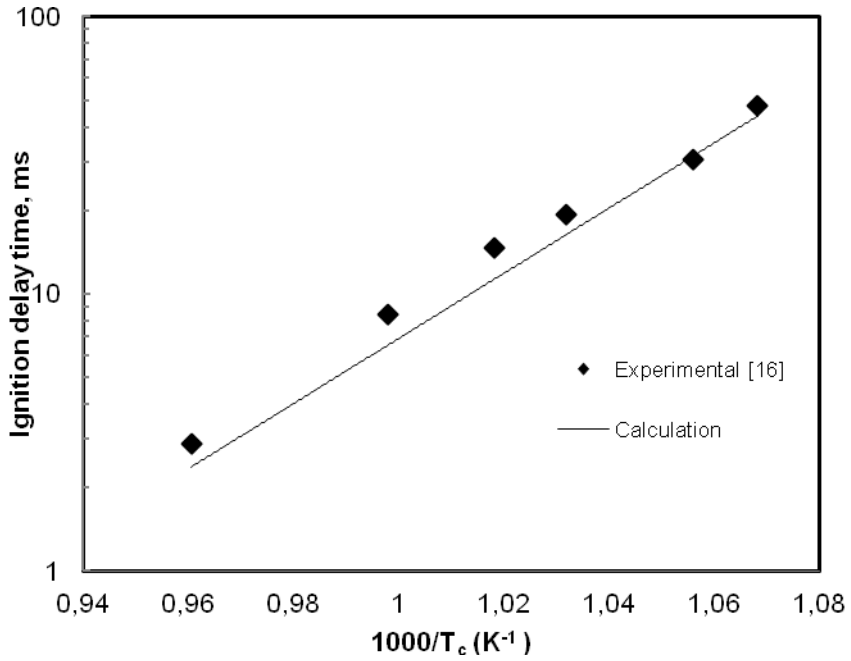

Figure 11. Measured (dots) and calculated (line) autoignition delay times as function of the reciprocal temperature for methanol/O_2/Ar mixtures at φ=0.25 and a pressure of P_c=15 bar. The measurements were performed by Kumar et al. [16].